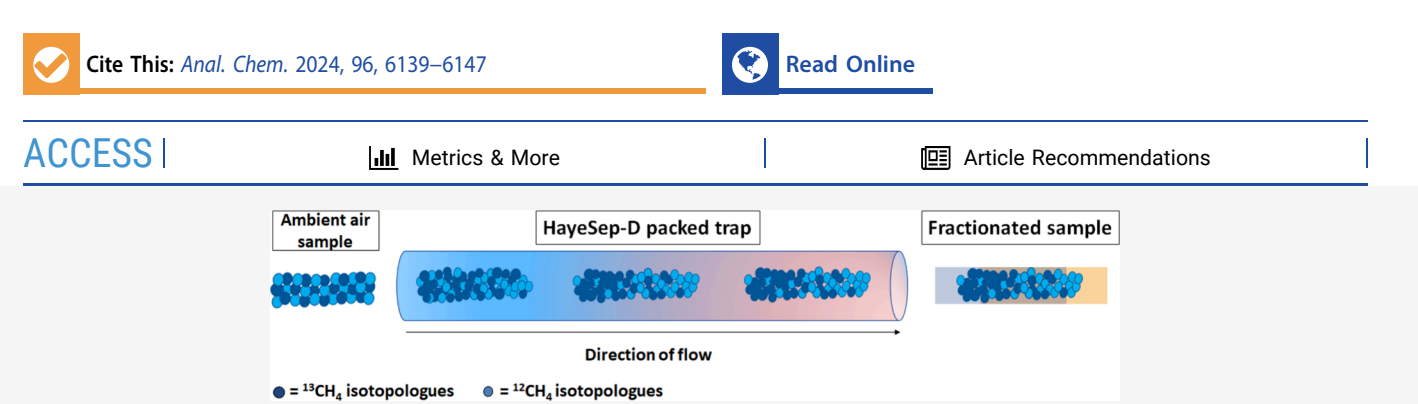
Fractionation of Methane Isotopologues during Preparation for **Analysis from Ambient Air**

Emmal Safi,* Tim Arnold, and Chris Rennick



ABSTRACT: Preconcentration of methane (CH₄) from air is a critical sampling step in the measurement of singly and doubly substituted isotopologue ratios. We demonstrate the potential for isotope fractionation during preconcentration onto and elution from the common trapping material HayeSep-D and investigate its significance in laser spectroscopy measurements. By altering the trapping temperature for adsorption, the flow direction of CH₄ through the trap and the time at which CH₄ is eluted during a desorption temperature ramp, we explain the mechanisms behind fractionation affecting $\delta^{13}C(CH_4)$ and $\delta^2H(CH_4)$. The results highlight that carbon isotope fractionation is driven by advection and diffusion, while hydrogen isotope fractionation is driven by the interaction of CH₄ with the adsorbing material (tending to smaller isotopic effects at higher temperatures). We have compared the difference between the measured isotope ratio of sample gases (compressed whole air and a synthetic mixture of CH4 at ambient amount fraction in an N2 matrix) and their known isotopic composition. An open-system Rayleigh model is used to quantify the magnitude of isotopic fractionation affecting measured $\delta^{13}C(CH_4)$ and $\delta^2H(CH_4)$, which can be used to calculate the possible magnitude of isotopic fractionation given the recovery percentage. These results provide a quantitative understanding of isotopic fractionation during the sample preparation of CH₄ from ambient air. The results also provide valuable insights applicable to other cryogenic preconcentration systems, such as those for measurements that probe the distribution of rarer isotopologues.

1. INTRODUCTION

Downloaded via PHYSIKALISCH-TECHN BUNDESANSTALT on November 26, 2025 at 13:15:50 (UTC). See https://pubs.acs.org/sharingguidelines for options on how to legitimately share published articles.

Methane (CH₄) is the second most significant anthropogenic greenhouse gas after carbon dioxide (CO₂). Globally, the amount fraction has increased from 0.72 ppm in preindustrial times to 1.9 ppm in 2021. Emissions need to be reduced with urgency; however there is significant uncertainty surrounding the relative strength and the spatial and temporal variability of specific sources and sinks.²⁻¹² As well as renewed growth of CH_4 amount fractions, the global $\delta^{13}C(CH_4)$ trend has shifted to more negative values, with a total globally averaged shift of approximately 0.3% between 2007 and 2019.5 This isotope ratio of atmospheric CH₄ is driven by the isotopic signature and magnitude of specific sources and the fractionation processes of atmospheric removal. Different sources have characteristic isotopic ratio signatures; for example, biogenic CH₄ samples from sources such as wetlands and landfill sites are isotopically lighter in $\delta^{13}C(CH_4)$ than pyrogenic or thermogenic fossil sources. ¹³ Increased measurements on a continuous basis of both isotopic signatures of sources and the atmosphere are needed to improve our understanding of the CH₄ budget.

Currently, the prevailing technique for high precision measurements of the CH₄ isotope ratio in ambient air is isotope ratio mass spectrometry (IRMS). 14-20 IRMS allows for very precise measurements; however, this is predominately a laboratory-based technique where samples are collected using flasks and brought back to the laboratory.²¹ Most recently, however, semicontinuous, in situ measurements of $\delta^{13}C(CH_4)$ and $\delta^2 H(CH_4)$ have been made by IRMS. These measurements have shown where the discrepancies between measurements and models lie in terms of the accuracy of emission inventories, demonstrating the potential of continuous, high temporal resolution CH₄ isotope ratio data.²² The caveat to IRMS, however, is the analysis of the two major isotope ratios in CH₄ require different instruments and preparation techniques: combustion to CO_2 for $\delta^{13}C(CH_4)$ and pyrolysis for $\delta^2 H(CH_4)$, where operation of such an instrument requires significant investment related to ongoing maintenance.

Received: October 30, 2023 Revised: March 1, 2024 Accepted: March 4, 2024 Published: March 22, 2024





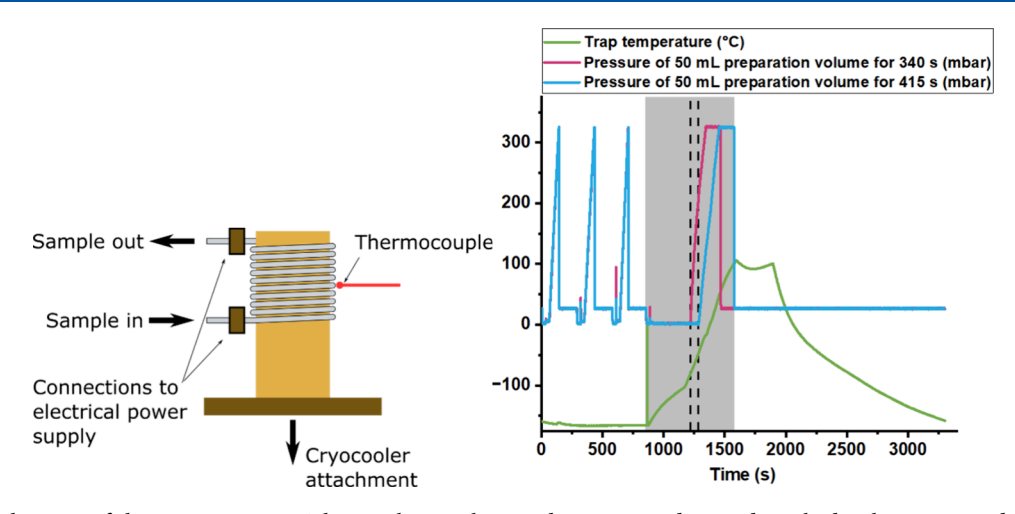


Figure 1. Left: Schematic of the trap on Boreas. The stainless-steel trap tubing is wound around a cylindrical copper standoff. The standoff is attached to a baseplate that is connected to the cryocooler. The trap temperature is monitored via a pair of thermocouples affixed to both the trap tubing and the inside of the standoff, located halfway down the trap, as shown by the red line. Right: Stripchart of the trap temperature shown by the green trace (measured by the thermocouple attached midway on the outside of the trap tubing); the shaded region indicates the start and end of the temperature ramp. The green and pink traces show the preparation volume pressure for two different instrument "runs" for the earliest and latest delay times used in this work. The vertical dashed lines represent the delay times from two different runs (340 and 415 s), set relative to the start of the temperature ramp indicating the valve opening time allowing the sample to transfer from the trap to the preparation volume.

Optical isotope ratio spectroscopy (OIRS) has shown a strong potential to be able to provide high-frequency measurements with lower maintenance requirements. However, these instruments have not been shown to match the precision from typical IRMS methods due to poor signal-tonoise ratio caused by the low abundance of CH4 in ambient air. 23,24 For this reason, laser spectrometers have been paired with preconcentrator systems to concentrate the CH₄ from air and increase the signal levels. The potential for these systems for continuous field measurements of $\delta^{13}C(CH_4)$ and $\delta^2 H(CH_4)$ has been demonstrated by Eyer et al.²³ precision of 0.19% for $\delta^{13}C(CH_4)$ and 1.9% for $\delta^{2}H(CH_4)$ and more recently by Rennick et al.²⁴ with precisions of 0.07% for $\delta^{13}C(CH_4)$ and 0.9% for $\delta^{2}H(CH_4)$. The typical precision of IRMS methods is <0.05% for $\delta^{13}C(CH_4)$ and 1% for $\delta^2 H(CH_4)$. However, preconcentration comes with its own set of challenges in terms of the large volumes of sample needed for analysis, i.e., separation of CH₄ from bulk and other traces gases in ambient air. 23,24 Incomplete transfer of CH₄ from the preconcentrator to the spectrometer not only decreases the total amount but also potentially introduces significant bias in measured isotope ratio. This is due to physical isotopic fractionation processes occurring during both adsorption and desorption during the preconcentration process. Near-complete capture is therefore essential to limit the fractionation effects influencing the measured $\delta^{13}C(CH_4)$ and $\delta^2 H(CH_4)$ values.²³

The porous polymer adsorbent HayeSep-D is universally accepted as a packing material for the preconcentration of stable volatile chemical species from ambient air. The use of HayeSep-D allows for an increase in the detection limit and removal of interferences for analysis of trace gases and less abundant isotopes. ^{15,17,19,24,26–28} Apart from HayeSep-D, other adsorbents are also used to preconcentrate CH₄ from ambient air, such as activated charcoal. ^{28–30} In this paper we investigate fractionation during the various phases in the preconcentration instrument Boreas, introduced by Rennick et al. ²⁴ We use this system to show that the separation process has the potential to induce fractionation effects and to quantify

these effects under various instrument operating conditions. We show how trapping temperatures influence fractionation effects and how a HayeSep-D based trapping system can be optimized to limit these effects.

2. METHODS

2.1. Instrument Description. A full description of Boreas including the design and operating parameters is given in Rennick et al.²⁴ Briefly, Boreas samples ~5 L of ambient air via a sampling pump. The sample is dried using a Nafion dryer before entering the cryogenic trap. The trap is a 1.5 m long, 1/8 in. outside diameter stainless steel tube with the central 1 m length packed with a total of 1.6-2.4 g of HayeSep-D porous polymer graded to 100/120 mesh and held in place with quartz wool plugs (Restek, USA). HayeSep-D is a high purity macroporous divinylbenzene resin that is widely used for separation of light gases in gas chromatography. It has also been used for cryogenic preconcentration of halogenated trace gases, 26,27 nitrous oxide (N₂O), 31 CH₄, 23,24,28 and more recently CH₄ from large sample volumes using a second, smaller HayeSep-D refocusing trap.³² Most of the trap tubing is helically wound onto a hollow copper standoff that is cooled by a Cryotel GT Stirling Cryocooler (CryoTel GT Sunpower Inc., USA); the trap configuration is shown schematically in Figure 1. Temperature is measured by temperature controllers (Omega Engineering CNi32) recording the output of two type-E thermocouples attached inside the standoff and to the outside of the trap tubing by thermally conductive epoxy (Omegabond 101, Omega Engineering). The tubing temperature is used as a reference point for the repeatability of the trap temperature and does not account for temperature gradients between the ends closest to and furthest from the cryocooler head. It also does not account for hot- and coldspots arising from differing contact pressures between the tubing and standoff. This measurement is taken to be representative of the HayeSep-D temperature, for tracking variations between consecutive runs of the standard and air, and is referred to as the "trap temperature" here. Trap and standoff temperatures for the chosen Stirling temperature set

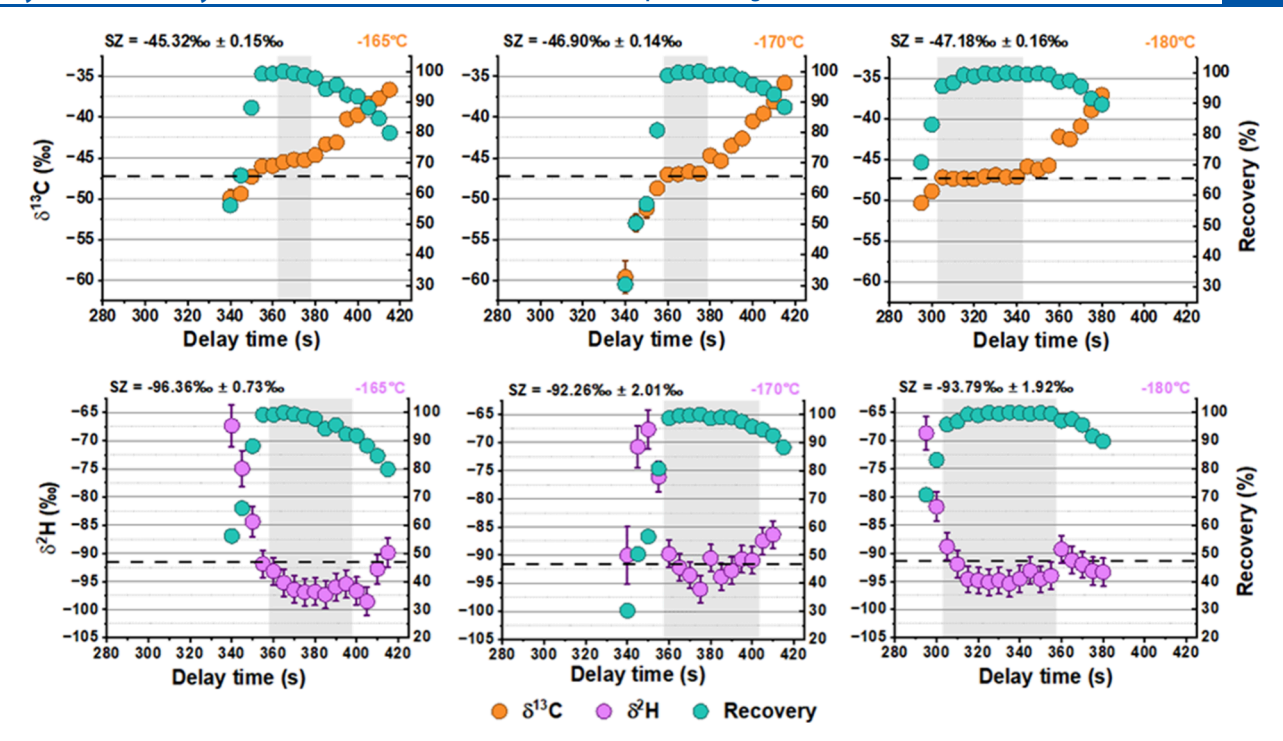


Figure 2. Top: Variation in the isotope ratio $\delta^{13}C(CH_4)$ with delay time (set relative to the start of the temperature ramp indicating the valve opening time allowing the sample to transfer from the trap to the preparation volume). The shaded region matches the delay times at which largest amount of transfer of the CH₄ sample is seen in the amount fraction data, i.e., the "stability zone" (SZ). The average value of the SZ is indicated in the plots. Bottom: Variation in the isotope ratio $\delta^2H(CH_4)$ with delay time. Note that for the top and bottom panels, plots are recorded for trapping temperatures of -165 °C, -170 °C, and -180 °C respectively. The percentage of CH₄ captured (the recovery) in each delay scan run is also indicated in the plots. The black dashed line represents the original isotopic composition of the sample gas used (for $\delta^{13}C(CH_4)$ it is -47.3%0 $\pm 0.1\%$ 0, and for $\delta^2H(CH_4)$ it is -91.5%0. Where the error bars cannot be seen, they are smaller than the plotted points.

points shown in Figure 2 are listed in Table 1. The trap temperature repeatability is better than 1 K at time points

Table 1. Corresponding Trap Temperature and Standoff Temperature for the Individual Stirling Set Temperature for the Data That Are Shown in Figure 2^a

| Stirling set point (°C) | trap temperature (°C) | standoff temperature ($^{\circ}$ C) |
|-------------------------|-----------------------|--------------------------------------|
| -165 | -135.0 | -143.6 |
| -170 | -158.8 | -168.8 |
| -180 | -159.4 | -169.6 |

^aThe trap temperature is taken from an E-type thermocouple attached to the outside of the trap tubing. The standoff temperature is taken from an E-type thermocouple attached to the inside of the copper standoff.

compared across instrument cycles. A stripchart showing the temperature profile of the trap is shown in Figure 1.

2.2. Trapping and Sample Transfer. The sample enters the trap tubing at the end closest to the cryocooler and flows at an average rate of ~ 500 mL min⁻¹ for 540 s, with the trap continuing to cool without any active heating. After the trapping phase, the trap is allowed to depressurize, the valve system then switches to a flow of pure nitrogen at 6 mL min⁻¹ while the trap is slowly heated for 720 s.

The trapping temperature during CH_4 adsorption onto the trap is dictated by the set point temperature of the cryocooler at the end of the previous run. In addition to stepwise heating of the trap during the run cycle (shown in Figure 1 by the shaded region), it is also therefore essential to ensure that this temperature, as determined by the cryocooler set point, is

optimized. Note that after trapping, the same temperature ramp profile is used for elution irrespective of trapping temperature. When the set point leads to a colder trap (high power, quicker heat removal) at the end of a cycle then trapping on the subsequent run will experience the onset of freezing of the more volatile bulk gases. This makes it challenging to achieve reproducible starting conditions for each run cycle. Conversely, if the cryocooler set point leads to a warmer trap (lower power, slower heat removal) at the end of a run cycle, it will lead to repeatable starting conditions. However, nonquantitative capture of the CH₄ from the sample gas becomes more likely due to the spreading of the CH₄ along the trap (as discussed in section 3.1) and subsequent contamination of the sample by N2O. This is due to the coelution of N2O from the trap with CH4 as a longer valve opening time will be needed for quantitative capture of the sample. During instrument optimization, an experiment was conducted involving delay scans at two distinct trapping temperatures. The thermocouple on the outside of the trap tubing recorded −135 °C for the first delay scan and −155 °C for the second. The maximum amount of N2O measured at -135 °C was 72% higher than that measured at −155 °C suggesting more N2O was eluting at the higher trapping temperature. Note that the temperature is not actively controlled during trapping but depends on the residual heat load through the wiring and tubing balanced by the heat removed by the cryocooler. The final temperature is controlled by the cryocooler set-point and has been found to produce a more repeatable temperature profile from run-to-run. This also eliminates the temperature spikes caused by the power supply

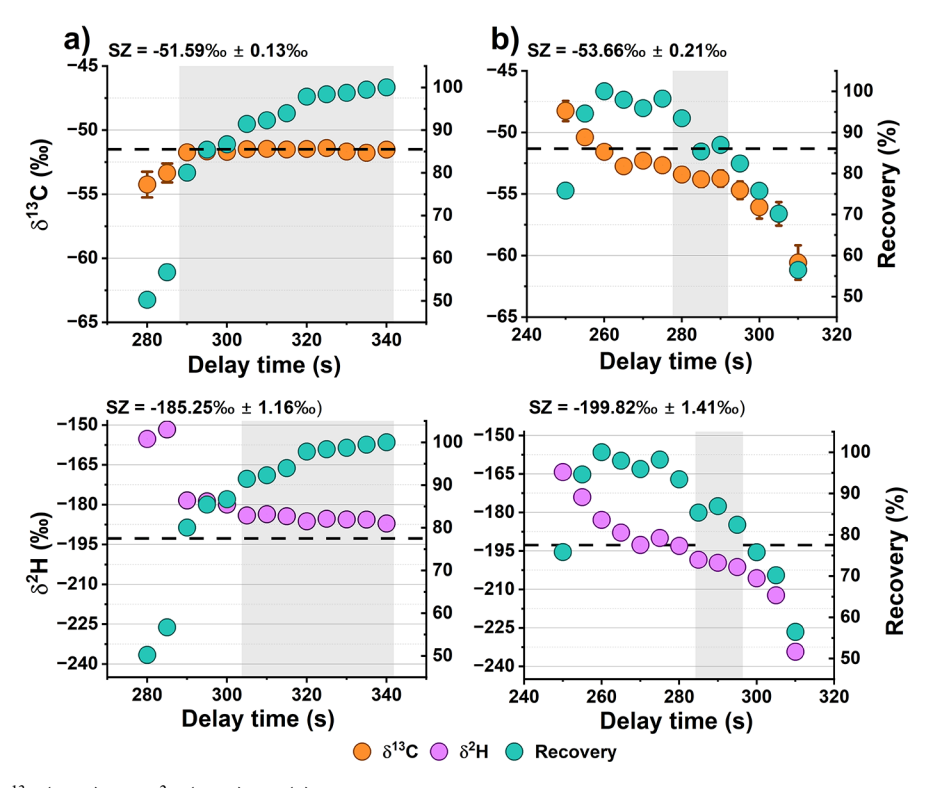


Figure 3. Variation in $\delta^{13}C(CH_4)$ and $\delta^2H(CH_4)$ for (a) forward flow direction when the sample can migrate along the trap tubing and (b) reverse flow direction when the trap direction is changed and the CH_4 sample can enter the preparation volume, without migrating through the trap. The difference in the average values of isotope ratios of the SZ compared to those in Figure 2 is due to the origin of the CH_4 source being different. The black dashed line represents the original isotopic composition of the sample gas used (for $\delta^{13}C(CH_4)$ it is $-51.5\%c \pm 0.04\%c$, and for $\delta^2H(CH_4)$ it is $-189.1\%c \pm 1.55\%c$). The percentage of CH_4 captured (the recovery) in each delay scan is also indicated in the plots. Where the error bars cannot be seen, they are smaller than the plotted points.

switching when using proportional integral derivative (PID) feedback temperature control.

The CH₄ is flushed through the trap following initiation of a temperature ramp to remove bulk gases, such as oxygen (O₂) and nitrogen (N2), before elution of CH4 into a 50 mL preparation volume, referred to as the "sample volume" in Rennick et al.²⁴ (Swagelok stainless steel miniature sample cylinder), prior to transfer to the 500 mL high-resolution duallaser direct absorption instrument (Aerodyne Research, Inc., TILDAS-FD-L2) cell. The transfer is controlled by a series of carefully timed valve changes to direct predominantly the CH₄ and N2 carrier gas to the spectrometer, with the eluant before and after this directed to vent. The pink and blue profiles in Figure 1 show the spectrometer preparation volume pressure as sample enters from the trap (start of filling is denoted by the dashed lines). The three preceding spikes in pressure (from 60 to 700 s) represent the spectrometer calibration standards filling the preparation volume which occur at the same time in every run cycle. The "delay time" variable is set relative to the start of the temperature ramp and the timing is optimized in a series of repeated trapping cycles with the delay time systematically changed from run to run. Figure 1 shows both the earliest and latest delay times (i.e., 340 and 415 s after the start of the temperature ramp). In cycles where the valve opening (delay time) is too short, the valve will close before all CH₄ has eluted and the trailing edge of the CH₄ peak is directed to the vent. When the delay time is too late, then the leading edge of CH₄ elution is directed to vent and only the trailing edge is loaded into the spectrometer. At an optimal delay time, the complete eluted CH₄ peak is transferred to the

spectrometer. The delay time before opening is optimized and set as an experimental parameter; however, the closing is set automatically by a pressure set point (320 mbar) measured in the preparation volume. The fill time typically takes around 150 s but is shorter at earlier delay times, when the trap temperature is still low, and residual bulk gases are released from the HayeSep-D, therefore increasing the effective flow rate. The spectrometer is used in batch mode during normal trapping to transfer the sample to the 500 mL cell. Batch mode enables the cell to hold the sample for a 100 s averaging interval. The spectrometer can, in principle, also operate in a continuous flow mode where the sample is continuously pumped through the cell. However, the slow flow rate of the sample from the trap to the cell (during elution) would result in a very low cell pressure. The spectrometer would then need to adjust the sample flow to stabilize the cell pressure causing variations in the trap flow rate. This would therefore be different to the standard flow conditions of the elution into the evacuated preparation volume, potentially changing observed fractionation effects.

The delay time is varied in increments of between 5 and 20 s between each run, with all other parameters identical. Figure 2 shows the results from a set of experiments as a plot of $\delta^{13}C(CH_4)$ (top panel) and $\delta^2H(CH_4)$ (bottom panel) as functions of the delay time (in 5 s intervals). This shows that there is an optimum delay time where there is complete transfer of captured CH_4 as indicated by the shaded region. These shaded regions, i.e., the stability zone (SZ), are taken to be where the repeatability on $\delta^{13}C(CH_4)$ measurements is $\leq \pm 0.20\%$ and $\leq \pm 2.0\%$ for $\delta^2H(CH_4)$. Once the CH_4 has

eluted, the trap is flushed to the vent. Once 100 $^{\circ}$ C is reached, it remains at this temperature for 300 s to allow purging of less volatile gases (primarily H_2 O). The heating is then stopped, and the trap is allowed to cool passively ready for the next run. After the eluted CH_4 is transferred to the preparation volume, the sample is passed to a 500 mL cell for the isotopologue abundance to be measured. After measurement, the preparation volume and 500 mL cell are evacuated and filled with synthetic standards for instrument calibration.

2.3. Calibration and Assignment of Isotope Ratios. The measured isotopologue amount fractions are calibrated using primary reference mixtures (PRMs) prepared by gravimetry from pure CH₄ that is referenced to the VPDB and VSMOW scales for δ^{13} C and δ^{2} H respectively. The calibration strategy for both amount fraction and isotope ratio for the Boreas preconcentrator is detailed in Rennick et al. Uncertainties on the isotope ratios in this study arise from contributions from both the instrument precision and the uncertainty in the calibration.

Rennick et al.²⁴ have previously assessed the spectrometer's linearity across a range of amount fractions using primary reference materials (PRMs). Two high amount fraction PRMs with CH₄ in pure N₂ were used as low and high calibration standards, and two additional PRMs were used for validation. These calibrate the instrument for each isotopologue fraction with the isotope ratio subsequently calculated. This calibration approach therefore inherently corrects the amount fraction dependence that has been seen with other calibration approaches. The calibration standards and one validation PRM (same parent CH₄) were prepared to concentrations of 500, 550, and 626 μ mol mol⁻¹ in pure N₂, while a second validation PRM (different parent) was prepared to 600 μ mol mol⁻¹ in pure N₂. The linearity of the spectrometer has previously been verified over this range and up to 750 μ mol mol⁻¹, validating the two-point isotopologue calibration scheme.²⁴ Some measurements presented here fall below the lowest PRM, so we calibrate these measurements by extrapolation, and the larger uncertainty is represented in the error bars in Figures 2, 3, and 4.

The sample gas for the experiments (called Boreas target, abbreviated to BT) is taken from either (a) compressed whole air reference gas filled at the Mace Head Observatory, Ireland, using an oil free compressor following the National Oceanographic and Atmospheric Administration (NOAA) procedures for certified reference materials involving processes of cylinder conditioning and venting before a final fill to ~200 bar, 33 or (b) a single synthetically made reference gas of 1.8 μ mol mol⁻¹ of CH₄ in pure N₂ prepared gravimetrically by diluting a parent mixture of 2.2% CH₄ in N₂ (N6.0, CK gases). The isotopic composition of the whole air is $\delta^{13}C(CH_4) = -47.3\%e \pm 10^{13}$ 0.1% and $\delta^2 H(CH_4) = -91.5\%$ $\pm 0.6\%$ and for the synthetic reference gas is $\delta^{13}C(CH_4) = -51.5\%0 \pm 0.04\%0$ and $\delta^2 H(CH_4) = -189.1\% \pm 1.55\%$. IRMS analysis for $\delta^2 H(CH_4)$ was not possible for the compressed whole air standard, and the value is derived from a tank comparison with a second compressed whole air standard. The $\delta^2 H(CH_{\perp})$ for the second compressed whole air standard was estimated from the NOAA-INSTAAR record for 2005-2009 by Rennick et al.24

The Boreas trap eluant was previously collected under optimized conditions and analyzed to identify other major contaminating gases. ²⁴ These gases can be concentrated and eluted alongside CH₄ but would not be detectable by the laser

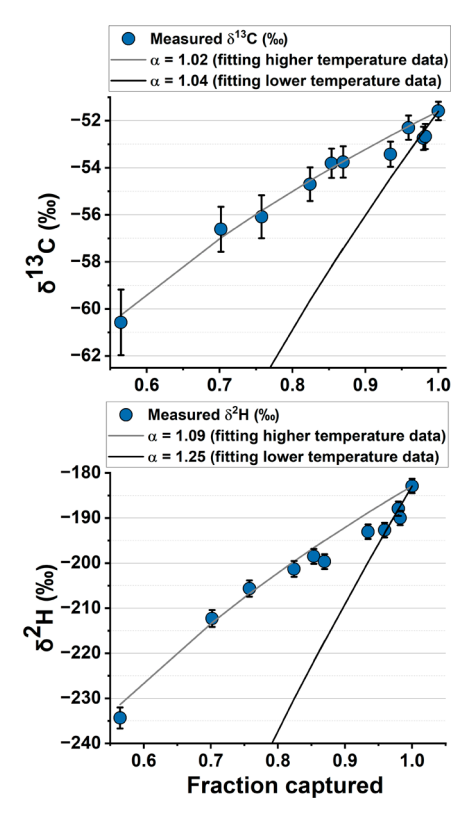


Figure 4. Variation of (a, top) $\delta^{13}C(CH_4)$ and (b, bottom) $\delta^2H(CH_4)$ with fraction of sample captured for reverse flow during elution of the trailing edge of CH_4 . The data are fitted using the Rayleigh model in eq 1. Gray lines model a smaller isotopic fractionation and black lines a larger isotopic fractionation. The delay time in seconds for the first and last runs in the plot from the delay scan is also indicated.

spectrometer. In the previous study, the O₂ amount fraction from Boreas was determined by comparing it to National Physical Laboratory (NPL) in-house standards, resulting in a calculated value of 10 mmol mol⁻¹. This results in a 0.12% offset in $\delta^{13}C(CH_4)$ relative to O_2 -free standards, assuming the same proportionality seen in other studies.²³ While standardized procedures for isotope ratio offsets have not been established, this remains a current focus of interest within the metrology community. In the meantime, under normal operating conditions, we adopt a practice of measuring our BT between every sample gas run and subsequently apply an offset to the data, ensuring compatibility with at least one IRMS measurement. The typical reported repeatability on Boreas is determined by a 4-point rolling standard deviation of BT, yielding a value of 0.048% for δ ¹³C(CH₄). When accounting for the offset correction related to O_2 , the propagated standard uncertainty of $\delta^{13}C(CH_4)$ for a sample gas measurement is 0.070%o.

3. RESULTS AND DISCUSSION

3.1. Fractionation of ¹³CH₄ and ¹²CH₄. Figure 2 shows the variation of the measured $\delta^{13}C(CH_4)$ with delay time for three different trapping temperatures during the sampling of BT. The top panel of Figure 2 shows a fractionation effect in $\delta^{13}C(CH_4)$ where the eluted CH_4 sample is isotopically lighter at early delay times and heavier at later delay times. At the optimum delay times, the aim is quantitative recovery of CH_4 from the trap, therefore preventing any isotopic fractionation.

At times earlier or later than this optimum the CH_4 recovery decreases, indicating loss of sample during the transfer, and a change in the measured $\delta^{13}C(CH_4)$ and $\delta^2H(CH_4)$. At colder trapping temperatures, the SZ extends over a larger range of delay times, shown as the shaded regions in Figure 2. This indicates that the duration of CH_4 elution is shorter with respect to the window of time between valve opening and closing, i.e., a narrower CH_4 elution peak.

The CH₄ (and other less volatile species) will adsorb to the trapping material in equilibrium with the gas phase. The rate at which CH₄ moves through the trap during trapping and elution can be approximated in a similar form to the two-phase model of gas chromatography.³⁴ CH₄ is strongly bound to the HayeSep-D (i.e., stationary phase), and the flow of bulk gases acts as a carrier gas driving advection-diffusion. During elution, the carrier gas is changed to the slow flow of pure N₂, and the increased temperature moves the CH₄ equilibrium into the gas phase. At higher trapping temperatures, the equilibrium between the adsorbed and gaseous phases of CH₄ moves towards the gas phase, and the rate of transport through the trap increases. This results in a wider elution peak that causes the effect seen in Figure 2 where the stability region is shorter for higher trapping temperatures.

The variation in $\delta^{13}C(CH_4)$ of the eluted CH_4 arises from small differences in the transport rate of the $^{12}\text{CH}_4$ and $^{13}\text{CH}_4$ isotopologues during both trapping and elution. Given the difference in mass between ¹²CH₄ and ¹³CH₄ isotopologues, variation in $\delta^{13}C(CH_4)$ with delay time and trapping temperature is likely driven by the mass dependence of the diffusivity. ¹²CH₄ and ¹²CH₃²H differ in both mass and the hydrogen isotope available to interact with the HayeSep-D surface, so a more complex variation in $\delta^2 H(CH_4)$ with delay time and trapping temperature could be expected. This is due to differences in both diffusivity and the nature of the adsorption interaction (section 3.2). The fractionation in carbon isotopes observed at the leading and trailing edges of the CH₄ elution peak can be conceptually described in terms of transport of CH4 through the packed trap tubing during the two experimental phases of trapping and elution. The variation of the diffusivity D for gases with temperature and molecular weight is approximated for gases by the Chapman-Enskog equation.³⁵ This predicts that the diffusivity for ¹³CH₄ in N₂ is 2% lower than for ¹²CH₄ under the conditions expected in the trap tubing. Because lighter ¹²CH₄ isotopologues are transported by the carrier gas more rapidly than the ¹³CH₄ isotopologues, there is fractionation at the leading and trailing edges of the elution peak. This results in a more negative $\delta^{13}C(CH_4)$ measured at short delay times and a more positive value measured at longer delay times. It is important to note that this is not chemical fractionation as no CH₄ is produced or consumed.

At -165 °C only a small SZ is evident, and the measurements are all shifted to heavier values (the value of $\delta^{13}C(\text{CH}_4)$ of the compressed whole air is -47.3% \pm 0.10%). This is likely due to a significant proportion of CH₄ eluting before the earliest delay time used in this set of experiments. There is, however, still a plateauing of the measurement at ~365 s owing to the majority of CH₄ eluting around this time, albeit with a heavier average ratio. The isotopic SZs at -170 and -180 °C are clear and very close to the isotopic composition of the original sample gas. The isotopic composition of the SZ of the -180 °C experiment is not significantly different to that of the sample gas (within the

standard error). The $-170~^{\circ}\mathrm{C}$ experiment shows a significant difference of 0.40%, toward heavier values, compared to the sample gas. This is again likely due to a small fraction of the CH₄ eluting before the earliest delay time. The SZs for the experiments span three delay scan runs for the $-165~^{\circ}\mathrm{C}$ compared to four for the $-170~^{\circ}\mathrm{C}$ and eight for the $-180~^{\circ}\mathrm{C}$ experiments. We verified that CH₄ had not broken through during trapping by conducting experiments at very early delay times (150–200 s). At the earliest delay time, when the trap flow was in the same direction for trapping and elution, no CH₄ could be detected. This indicates that only negligible amounts could be lost earlier in the instrument cycle, i.e., during trapping.

As explained in previous work by Eyer et al.²³ and Rennick et al.,²⁴ the coelution of the bulk gases with CH₄ can cause matrix effects in spectroscopic measurements of the isotope ratios of carbon. Figure 3a shows that the general behavior of fractionation of isotopes from the synthetic mixture (CH₄ in pure N₂) is very similar to that of CH₄ from BT shown in Figure 2. The average value of δ^{13} C(CH₄) of the SZ differs in Figure 3a compared to Figure 2 as the CH₄ originates from a different source (certified values of δ^{13} C(CH₄) and δ^{2} H(CH₄) for the CH₄ in N₂ used in Figure 3a,b are $-51.5\%o \pm 0.04\%o$ and $-189.1\%o \pm 1.55\%o$ respectively).

The earlier delay times are when the majority of the bulk gases, i.e., N2 and O2, elute due to their lower boiling points relative to CH₄. Therefore, isotopic compositions measured at the earliest delay times are more likely to be affected by O2 interferences. For the experiments shown in Figure 2 (using a whole air matrix gas), the −165 and −180 °C runs had an offset of 2.6% and 3.3%, respectively, from the assigned isotopic composition of the compressed whole air for the earliest delay time (340 s and 295 s, respectively). The -170°C experiment saw an offset of 12.3% for the earliest delay time (340 s), however the recovery was only 30.3% compared to 56.2% and 70.8% for the -165 °C and -180 °C experiments, respectively. The larger offset is therefore attributed to fractionation effects due to the smaller amount of CH₄ recovered. Using a pure N₂ matrix gas, Figure 3a shows a similar CH₄ percentage recovery as the −165 and −180 °C experiments in Figure 2. At the earliest delay time (280 s) the CH₄ recovery using the pure N₂ matrix gas was 50.2% with a $\delta^{13}C(CH_4)$ value of -54.3%o. The fractionation seen in the earliest delay time in Figure 3a is due to the incomplete recovery of CH₄, as a pure N₂ gas matrix is used so eliminating O_2 interference. The $\delta^{13}C(CH_4)$ offset from the assigned value of the CH₄ N₂ is 3.2%. The offset observed for the pure N₂ gas matrix is only 0.1%0 larger than that seen in the -180 °C experiment using a compressed whole air matrix gas and is larger (by 0.6%) than the offset seen in the -165 °C experiment, again, with a whole air gas matrix. This indicates that the effects of the gas matrix (and therefore O₂ interferences) are insignificant in this study.

3.2. Fractionation of $^{12}\text{CH}_4$ and $^{12}\text{CH}_3^2\text{H}$. The measured variation in $\delta^2\text{H}(\text{CH}_4)$ with delay time is also plotted in Figure 2 (bottom panel). At short delay times the $\delta^2\text{H}(\text{CH}_4)$ values measured on the leading edge of the CH₄ peak are heavier, i.e., enriched in $^{12}\text{CH}_3^2\text{H}$; however, a lighter isotope signature is not evident on the trailing edge. The effect on the leading edge is the opposite to that observed for $\delta^{13}\text{C}(\text{CH}_4)$. The transport rate of CH₄ along the trap is influenced by the velocity of the carrier gas and the interaction strength of CH₄ with the stationary phase. For a purely mass-dependent physical

process, the speed of $^{12}\text{CH}_3{}^2\text{H}$ through the trap would be similar to $^{13}\text{CH}_4$ and both would show a similar trend in isotope ratio with delay time. However, it is the hydrogen atoms that have the adsorption interaction with the adsorption surface.

An isotopic fractionation effect is also seen in gas chromatography where the substitution of hydrogen with deuterium in a hydrocarbon leads to the molecule becoming less hydrophobic, more lipophilic, or polar.³⁶ Bermejo et al.³ used various chlorinated mixtures of dimethylbenzene and their deuterated counterparts separated via a capillary GC with different polarity stationary phases. Separation of CH₄ from ¹²CH₃²H has also been achieved on a GC column³⁸ and investigated for metal-organic framework layers and membranes.³⁹ In all outcomes, the deuterated product eluted from the column before the nondeuterated counterpart and was not affected by polarity of the stationary phase (i.e., the material of the GC column). This was attributed to the shorter internuclear distance in the ¹³C-²H versus ¹³C-¹H bond, leading to a more compact electron distribution and therefore a decrease in electronic polarizability. It has been suggested the inverse isotopic effect on noncovalent interactions is mainly due to the difference in length of the ${}^{13}C-{}^{1}H$ and ${}^{13}C-{}^{2}H$ bonds and to the changes in the physical properties of a molecule upon deuteration such as polarity and molecular volume.³⁶

This hypothesis of physisorption driving the isotopic fractionation can explain the stability (i.e., lack of heavier measurements at later delay times) in the $\delta^2 H(CH_4)$ measurements later in the elution profile. The later elutions occur at higher temperatures that would either (a) mobilize all remaining CH_4 into the gas phase irrespective of isotopic composition (equilibrium completely shifts to the gas phase) or (b) provide sufficient energy in the system to remove the kinetic barrier of desorption across all isotopologues.

3.3. Reverse Trap Flow. Under normal operating parameters, sample gases are directed through the trap from the end closest to the cryocooler, and reversal of flow only occurs after full elution of CH₄ in order to recondition the trap ready for the following run. To investigate the dominant fractionation influence, however, the CH₄ sample was introduced into the trap in the normal direction but flow direction was reversed for CH₄ elution (forward trapping, reverse elution) i.e., the CH₄ eluted without traveling through the trap. Due to the prevalent challenge of matrix and direct interferences on measurement of the isotopologues, the experiment was conducted with the synthetic mixture of CH₄ in a N₂ matrix. This was to enable the results to be unaffected by any potential matrix gas and spectral interferences, which could be introduced using a compressed whole air sample gas. In Figure 3 the delay scan for this reverse elution experiment shows the opposite trend of $\delta^{13}C(CH_4)$ with delay time compared to forward elution. Loading the sample into the spectrometer at early delay times results in a more positive $\delta^{13}C(CH_4)$, i.e., enriched in $^{13}CH_4$. This is evidence that the mass-dependent fractionation behavior of the ¹²CH₄ and ¹³CH₄ isotopologues is occurring during the trapping phase, rather than during the elution phase.

The enrichment with ¹²CH₃²H for the early eluted samples during reverse flow, however, is consistent with results from the forward flow experiments. At very late delay times, however, an enrichment in the lighter isotopologue is evident, unlike in the forward flow elution runs. As CH₄ does not need

to travel through the trap, it is eluted much faster during reverse flow directions when temperatures are significantly lower at earlier times in the temperature ramp. We hypothesize that at these lower temperatures during elution in the reverse direction, stronger isotopic fractionation is induced, which we attempt to describe quantitatively in section 3.4.

The average values of $\delta^{13}C(CH_4)$ and $\delta^2H(CH_4)$ in the stability zones differ between Figure 3a and Figure 3b. The offset is seen between the certified value $(-51.5\%e \pm 0.05\%e)$ and measured eluted CH₄ in Figure 3b. This again is likely due to a significant amount of CH4 eluting before the earliest delay time, as seen with the shift of $\delta^{13}C(CH_4)$ in Figure 2 for the −165 °C experiments. However, unlike with the forward flow direction, where the shift is toward heavier $\delta^{13}C(CH_4)$ values, the shift in $\delta^{13}C(CH_4)$ is toward lighter values for Figure 3b. This can be attributed to the fact that in the reverse direction, at earlier delay times, heavier sample will elute first, as it does not need to diffuse along the trap. The relative shift in the average value of the SZ for $\delta^2 H(CH_4)$ for Figure 3b is to lighter values, which is the same behavior observed for the −165 °C experiment in Figure 2. This is further evidence that for earlier delay times some CH4 has already eluted. The shift in $\delta^2 H(CH_4)$ to lighter values for both trap directions can best be attributed to a weaker adsorption of ¹²CH₃²H to the HayeSep-D.

3.4. Rayleigh Fractionation Model. The experimental results shown in Figures 2 and 3 are measuring either a) the CH₄ eluted from the trap first (with the remaining CH₄ still on the trap) or b) the CH₄ remaining on the trap (where the preceding CH₄ has eluted previously at earlier delay times). Therefore, the fractionation can be modeled by the Rayleigh equation as consisting of two reservoirs in an open system (once CH₄ leaves the trap the separation of gas phase and adsorbed phase is irreversible). The Rayleigh model is fitted to CH₄ in pure N₂ and under conditions of reverse flow during elution (Figure 3b). This experiment represents the most "ideal" trapping conditions with no interferences from bulk gases and reduced effects of fractionation during transport through the HayeSep-D column length.

We use the following form of the Rayleigh equation:⁴⁰

$$R_{\rm L} = R_0 f^{\alpha - 1} \tag{1}$$

where $R_{\rm L}$ is the isotope ratio ($^{13}{\rm C}/^{12}{\rm C}$ or $^{2}{\rm H}/^{1}{\rm H}$) measured for later delay times (i.e., of the CH₄ left on the trap), R_0 is the isotopic composition ($^{13}{\rm C}/^{12}{\rm C}$ or $^{2}{\rm H}/^{1}{\rm H}$) of the original starting material before any separation (that of the synthetic mixture of fossil-fuel derived CH₄ at ambient amount fraction in a N₂ matrix), f is the ratio of the amount remaining on the trap to the total starting amount of CH₄, and α is the fractionation factor.

At earlier delay times (where a portion of the trailing edge of the CH_4 peak is not captured) the two reservoirs are (i) the CH_4 transferred to the spectrometer (1-f) and (ii) the CH_4 remaining on the trap (f). At later delay times (where a portion of the leading edge of the CH_4 peak is not captured), the two reservoirs are (i) the CH_4 already eluted to vent before opening the spectrometer valve (1-f) and (ii) the CH_4 transferred from the trap to the spectrometer later in the temperature ramp (f). The CH_4 eluted to vent represents the CH_4 leaving the trap first, characterized by a lighter isotopic composition. This portion is vented as the spectrometer's valve remains closed off from measurement. Conversely, the CH_4 transferred from the trap to the spectrometer represents the

CH₄ remaining on the trap, characterized by a heavier isotopic composition. It would not have been measured had the spectrometer's valve been opened earlier, as it would have remained on the trap while the lighter material was eluting.

Figure 4 shows the Rayleigh model fitted to the experimental data from Figure 3b for the later delay times using eq 1. The data were fitted using fractionation factors for large fractionation (α further from 1) and small fractionation (α closer to 1). Particularly, for $\delta^2 H(CH_4)$ in Figure 4 it can be seen that earlier in the elution (when most of the CH_4 is captured, earlier delay time, f closer to 1) the measurements follow from a higher degree of isotopic fractionation (curve with $\alpha=0.8$); however, CH_4 later in the elution follows a less steep fractionation curve. This can be attributed to the effect of temperature on isotopic fractionation: earlier in the temperature ramp, the fractionation is larger as the temperature is lower.

4. CONCLUSIONS

We have investigated the fractionation of CH₄ stable isotopes in our cryogenic preconcentrator system for optical analysis of $\delta^{13}C(CH_4)$ and $\delta^2H(CH_4)$. We have quantified the fractionation effects observed during preconcentration onto and elution from a HayeSep-D packed trap, and the results identified a range of transfer times for three different trapping temperatures where quantitative transfer of samples is achieved. Incomplete transfer shows not only a lower amount fraction but also a systematic shift in the measured $\delta^{13}C(CH_4)$ and δ^2 H(CH₄). We describe this fractionation effect at the leading and trailing edges of the CH₄ elution peak. For δ^{13} C(CH₄) the leading edge is enriched in the lighter ¹²CH₄ isotopologue, in line with a kinetic diffusion driven effect. Explaining the fractionation affecting $\delta^2 H(CH_4)$ is more challenging as the mass-driven effects compete with the difference in adsorption bond strength of ¹²CH₃²H to the stationary phase compared to ¹²CH₄ which results in an apparent inverse isotopic effect than would be expected considering only the mass difference.

Additionally, we conducted comparisons between the measured isotope ratios of sample gases and their known isotopic composition, revealing insignificant effects of the gas matrix including O_2 interferences for the chosen delay times. Furthermore, utilizing an open-system Rayleigh model, we analyzed the $\delta^{13}C(CH_4)$ and $\delta^2H(CH_4)$ isotope ratio measurements of CH_4 in an N_2 matrix sample gas. This is done at different transfer times during reversed elution flow, and results show a greater fractionation during early CH_4 elution compared to later stages. These findings provide insights into the fractionation dynamics and gas matrix effects in preconcentration systems, contributing to our understanding of stable isotope ratio analysis methodologies.

For ambient air analysis, the use of laser based systems (with preconcentration sample preparation) to achieve high precision CH₄ isotope ratio analysis and high resolution IRMS measurements for multiply substituted CH₄ isotopologue ratios are growing analytical fields. ^{23,24,32,41,42} Both of these new areas of study rely on rigorous artifact-free sample preparation. This work highlights the tolerances for CH₄ recovery in cryogenic trapping systems when measuring isotopic ratios at high precision and suggests the mechanisms behind isotopic fraction which could help in the design of future sample preparation methods for minimizing isotopic fractionation before analysis.

AUTHOR INFORMATION

Corresponding Author

Emmal Safi — National Physical Laboratory, Teddington TW11 0LW, U.K.; ⊚ orcid.org/0000-0002-3202-001X; Email: emmal.safi@npl.co.uk

Authors

Tim Arnold — National Physical Laboratory, Teddington TW11 0LW, U.K.; School of GeoSciences, University of Edinburgh, Edinburgh EH8 9XP, U.K.; ⊙ orcid.org/0000-0001-9097-8907

Chris Rennick — National Physical Laboratory, Teddington TW11 0LW, U.K.; orcid.org/0000-0003-4993-0156

Complete contact information is available at: https://pubs.acs.org/10.1021/acs.analchem.3c04891

Author Contributions

The investigation was jointly conceptualized by E.S., T.A., and C.R. Boreas preconcentrator instrument was deployed and managed by E.S., T.A., and C.R. Formal data analysis was performed by E.S. and T.A. Acquisition of funding for the research was arranged by T.A. The research methodology was jointly developed by E.S., T.A., and C.R. E.S., T.A., and C.R. wrote the manuscript. Subsequent review and editing were performed by E.S., T.A., and C.R.

Notes

The authors declare no competing financial interest.

ACKNOWLEDGMENTS

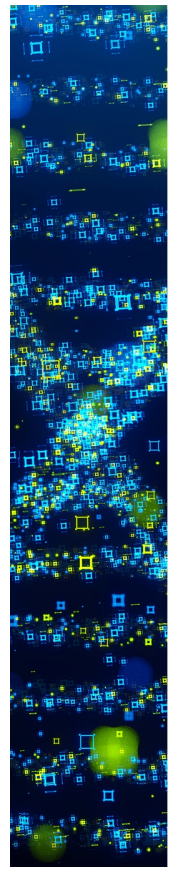
Gerry Spain is appreciatively acknowledged for his help filling compressed whole air standards at Mace Head Observatory. We thank Ruth Hill-Pearce, Eric Mussell-Webber, and Aimee Hillier for making the synthetic gas mixtures. Aerodyne Research Inc. has been very generous in helping us resolve any software issues when they arose. We acknowledge Peter Salameh of GCSoft for his support. Funding for this work is primarily through the NPL Directors' Fund, National Measurement System Funding, EMPIR STELLAR project, and the EURAMET 21GRD04 isoMET project. The 19ENV05 STELLAR project has received funding from the EMPIR program cofinanced by the participating states and from the European Union's Horizon 2020 research and innovation program. T.A. was supported by NERC grants NE/V007149/1 and NE/S003819/1.

■ REFERENCES

- (1) IPCC 2023. AR6 Synthesis Report: Climate Change 2023—IPCC. 2023. https://www.ipcc.ch/report/sixth-assessment-report-cycle/ (cited Aug 7, 2023).
- (2) Dlugokencky, E. J.; Nisbet, E. G.; Fisher, R.; Lowry, D. Philos. Trans. R. Soc., A 2011, 369 (1943), 2058-72.
- (3) Turner, A. J.; Frankenberg, C.; Wennberg, P. O.; Jacob, D. J. *Proc. Natl. Acad. Sci. U. S. A.* **2017**, 114 (21), 5367–72.
- (4) Rigby, M.; Montzka, S. A.; Prinn, R. G.; White, J. W. C.; Young, D.; O'Doherty, S.; et al. *Proc. Natl. Acad. Sci. U. S. A.* **2017**, *114* (21), 5373–7.
- (5) Nisbet, E. G.; Manning, M. R.; Dlugokencky, E. J.; Fisher, R. E.; Lowry, D.; Michel, S. E.; et al. *Global Biogeochem. Cycles* **2019**, 33 (3), 318–42.
- (6) Saunois, M.; Stavert, A. R.; Poulter, B.; Bousquet, P.; Canadell, J. G.; Jackson, R. B.; et al. *Earth Syst. Sci. Data* **2020**, *12* (3), 1561–623.
- (7) Lunt, M. F.; Manning, A. J.; Allen, G.; Arnold, T.; Bauguitte, S. J. B.; Boesch, H.; et al. *Atmos. Chem. Phys.* **2021**, 21 (21), 16257–76.

- (8) Stavert, A. R.; Saunois, M.; Canadell, J. G.; Poulter, B.; Jackson, R. B.; Regnier, P.; et al. *Global Change Biol.* **2022**, 28 (1), 182–200.
- (9) Basu, S.; Lan, X.; Dlugokencky, E.; Michel, S.; Schwietzke, S.; Miller, J. B.; et al. *Atmos. Chem. Phys.* **2022**, 22 (23), 15351–77.
- (10) Peng, S.; Lin, X.; Thompson, R. L.; Xi, Y.; Liu, G.; Hauglustaine, D.; et al. *Nature* **2022**, *612* (7940), 477–82.
- (11) Drinkwater, A.; Palmer, P. I.; Feng, L.; Arnold, T.; Lan, X.; Michel, S. E.; et al. Atmos. Chem. Phys. 2023, 23 (14), 8429-52.
- (12) Thanwerdas, J.; Saunois, M.; Berchet, A.; Pison, I.; Bousquet, P. Atmospheric Chemistry and Physics 2024, 24 (4), 2129-67.
- (13) Menoud, M.; van der Veen, C.; Lowry, D.; Fernandez, J. M.; Bakkaloglu, S.; France, J. L.; et al. Earth Syst. Sci. Data 2022, 14 (9), 4365–86
- (14) Lowe, D. C.; Allan, W.; Manning, M. R.; Bromley, T.; Brailsford, G.; Ferretti, D.; et al. *J. Geo. Res.: Atmospheres* **1999**, *104* (D21), 26125–35.
- (15) Fisher, R.; Lowry, D.; Wilkin, O.; Sriskantharajah, S.; Nisbet, E. G. Rapid Commun. Mass Spectrom. 2006, 20 (2), 200-8.
- (16) Bock, M.; Schmitt, J.; Behrens, M.; Möller, L.; Schneider, R.; Sapart, C.; et al. Rapid Commun. Mass Spectrom. 2010, 24 (5), 621–33.
- (17) Brass, M.; Röckmann, T. Atmos. Meas. Tech. 2010, 3 (6), 1707-21.
- (18) Bock, M.; Schmitt, J.; Beck, J.; Schneider, R.; Fischer, H. Atmos. Meas. Tech. 2014, 7 (7), 1999–2012.
- (19) Sapart, C. J.; van der Veen, C.; Vigano, I.; Brass, M.; van de Wal, R. S. W.; Bock, M.; et al. *Atmos. Meas. Tech.* **2011**, 4 (12), 2607–18.
- (20) Schmitt, J.; Seth, B.; Bock, M.; Fischer, H. Atmos. Meas. Tech. **2014**, 7 (8), 2645–65.
- (21) Röckmann, T.; Eyer, S.; van der Veen, C.; Popa, M. E.; Tuzson, B.; Monteil, G.; et al. *Atmos. Chem. Phys.* **2016**, *16* (16), 10469–87.
- (22) Menoud, M.; van der Veen, C.; Scheeren, B.; Chen, H.; Szénási, B.; Morales, R. P.; et al. *Tellus B* **2022**, *72* (1), 1823733.
- (23) Eyer, S.; Tuzson, B.; Popa, M. E.; van der Veen, C.; Röckmann, T.; Rothe, M.; et al. *Atmos. Meas. Techn.* **2016**, *9* (1), 263–80.
- (24) Rennick, C.; Arnold, T.; Safi, E.; Drinkwater, A.; Dylag, C.; Webber, E. M.; et al. *Anal. Chem.* **2021**, 93 (29), 10141–51.
- (25) Werner, R. A.; Brand, W. A. Rapid Commun. Mass Spectrom. **2001**, 15 (7), 501–19.
- (26) Miller, B. R.; Weiss, R. F.; Salameh, P. K.; Tanhua, T.; Greally, B. R.; Mühle, J.; et al. *Anal. Chem.* **2008**, *80* (5), 1536–45.
- (27) Arnold, T.; Mühle, J.; Salameh, P. K.; Harth, C. M.; Ivy, D. J.; Weiss, R. F. *Anal. Chem.* **2012**, 84 (11), 4798–804.
- (28) Eyer, S.; Stadie, N. P.; Borgschulte, A.; Emmenegger, L.; Mohn, J. Adsorption 2014, 20 (5), 657–66.
- (29) Espic, C.; Liechti, M.; Battaglia, M.; Paul, D.; Röckmann, T.; Szidat, S. *Radiocarbon* **2019**, *61* (5), 1461–76.
- (30) Sivan, M.; Röckmann, T.; Van Der Veen, C.; Popa, M. E. Extraction, purification, and clumped isotope analysis of methane (Δ ¹³ CDH $_3$ and Δ ¹² CD $_2$ H $_2$) from sources and the atmosphere. Gases/Laboratory Measurement/Instruments and Platforms; Oct 2023. https://egusphere.copernicus.org/preprints/2023/egusphere-2023-1906/ (cited Jan 23, 2024).
- (31) Mohn, J.; Guggenheim, C.; Tuzson, B.; Vollmer, M. K.; Toyoda, S.; Yoshida, N.; et al. *Atmos. Meas. Tech.* **2010**, 3 (3), 609–18.
- (32) Prokhorov, I.; Mohn, J. Anal. Chem. 2022, 94 (28), 9981-6.
- (33) U.S. Department of Commerce N. Global Monitoring Laboratory—Central Calibration Laboratory. https://gml.noaa.gov/ccl/airstandard.html. (cited Aug 1, 2023).
- (34) Romero, L. A.; Parks, M. L. On the two-domain equations for gas chromatography. Sandia National Laboratories (SNL), Albuquerque, NM, and Livermore, CA (United States); Jan 2009 Jan. Report No.: SAND2009-0605. https://www.osti.gov/biblio/978912 (cited Oct 28, 2023).
- (35) Fuller, E. N.; Schettler, P. D.; Giddings, J. C. Ind. Eng. Chem. 1966, 58 (5), 18-27.
- (36) Wade, D. Chemico-Biological Inter. 1999, 117 (3), 191-217.

- (37) Bermejo, J.; Blanco, C. G.; Guillén, M. D. J. Chromatogr. A 1986, 351, 425-32.
- (38) Bruner, F.; Canulli, C.; Corcia, A. D.; Liberti, A. *Nature Phys. Sci.* **1971**, 231 (25), 175–7.
- (39) Tian, Y.; Fei, W.; Wu, J. Ind. Eng. Chem. Res. 2018, 57 (14), 5151-60.
- (40) Mariotti, A.; Germon, J. C.; Hubert, P.; Kaiser, P.; Letolle, R.; Tardieux, A.; et al. *Plant Soil* **1981**, *62* (3), 413–30.
- (41) Chung, E.; Arnold, T. Global Biogeochem. Cycles 2021, 35 (10), No. e2020GB006883.
- (42) Haghnegahdar, M. A.; Sun, J.; Hultquist, N.; Hamovit, N. D.; Kitchen, N.; Eiler, J.; et al. *Proc. Natl. Acad. Sci. U.S.A.* **2023**, *120* (47), No. e2305574120.



CAS BIOFINDER DISCOVERY PLATFORM™

STOP DIGGING THROUGH DATA —START MAKING DISCOVERIES

CAS BioFinder helps you find the right biological insights in seconds

Start your search

